Ultrasonic Microplotting of Microgel Bioinks

Daniel Chester[1,2], Ponni Theetharappan[1], Terrika Ngobili[1], Michael Daniele[1,2,3], Ashley C. Brown[1,2,]*

1.Joint Department of Biomedical Engineering, University of North Carolina at Chapel Hill and North Carolina State University, Raleigh, NC

2. Comparative Medicine Institute, North Carolina State University, Raleigh, NC

3. Department of Electrical and Computer Engineering, North Carolina State University, Raleigh, NC

Key Words: Microgel, Microplotting, Patterned Films, Layer-by-layer fabrication, Bioink

Abstract: Material scaffolds that mimic the structure, function, and bioactivity of native biological tissues are in constant development. Recently, material scaffolds composed of microgel particles have shown promise for applications ranging from bone regeneration to spheroid cell growth. Previous studies with pNIPAm microgel scaffolds utilized a layer-by-layer (LBL) technique where individual, uniform microgel layers are built on top of each other resulting in a multilayer scaffold. However, this technique is limited in its applications due to the inability to control microscale deposition or patterning of multiple particle types within a microgel layer. In this study, an ultrasonic microplotting technique is used to address the limitations of LBL fabrication in order to create patterned microgel films. Printing parameters, such as bioink formulation, surface contact angle, and print head diameter, are optimized to identify the ideal parameters needed to

successfully print microgel films. It was found that bioinks composed of 2 mg/mL of microgels and 20% PEG by volume (v/v), on bovine serum albumin (BSA)-coated glass, with a print head diameter of 50 μm resulted in the highest quality prints. Patterned films were created with a maximum resolution of 50 μm with the potential for finer resolutions to be achieved with alternative bioink compositions and printing parameters. Overall, ultrasonic microplotting can be used to create more complex microgel films than is possible with LBL techniques and offers the possibility of greater printing resolution in 3D with further technology development.

Introduction:

The aim of the regenerative medicine field is to restore the original form and function of a damaged tissue; there have been numerous investigations into processes that allow for the creation of a material scaffold that can fulfill that role. The purpose of these material scaffolds is not only to provide a structure in which the regenerative process can take place, but also to participate in the regenerative process by providing pro-regenerative cues to cells migrating into the damaged tissue. Such cues can include the scaffold's mechanics, the scaffold's topography, and the inclusion of bio-active agents into the scaffold[1]. Recently, scaffolds composed of microgel particles have been investigated for use in regenerative medicine applications due to their high degree of tuneability which allows for their fine control over scaffold properties and, therefore, utility in a multitude of applications[2]. These applications can range from creating a matrix for bone regeneration[3], encapsulating cells for spheroid growth[4], and creating patient specific scaffolds for auricular cartilage regeneration[5].

Microgels are micro or nanometer-sized colloidal hydrogels that can be made responsive to external stimuli. These colloidal particles can be used as building blocks in assemblies wherein the material properties of individual microgels affect bulk properties of microgel-based materials,

suspensions, and mixtures[6–9]. Extremely sophisticated, multi-responsive systems can be built by combining different microgel building blocks, allowing for a "plug and play system" with high levels of control over design parameters. Importantly, microgel-based materials have the potential to modulate cellular behavior through exquisitely tuned spatial, energetic, temporal, and molecular properties[7,9], and microgel-based materials provide an unparalleled level of control over material properties, such as mechanics and degradation rates, compared to bulk gels with the same polymer composition. Therefore, microgels are an attractive building block for creating scaffolds for tissue engineering purposes.

Microgels have widely been synthetized from synthetic polymers[10–12], perhaps the most well studied of which is poly N-isopropylacrylamide (pNIPam). pNIPam microgel assemblies created through layer-by-layer (LBL) fabrication processes have been well characterized[6]. Using this technique, microgel films have successfully been developed to control cell attachment/detachment from scaffolds[13], facilitate drug delivery[14], act as antimicrobial coatings[15], and direct cell migration dynamics through mechanical cues[16]. While LBL techniques for creating microgel films have widely been successful at creating uniform films, one major limitation of the technique is that it offers no spatial control over the deposition of the microgel particles. Current LBL techniques also do not allow for the creation of more complicated scaffolds containing multiple particle types in defined locations.

In order to overcome the limitations presented by LBL techniques, microgels have been adapted for 3D printing applications to create more defined and complex scaffolds. As such, extrusion-based 3D printing technique have become a popular method by which microgel bioinks are printed[17–22]. In order to print through extrusion-based printing methods, microgel bioinks are loaded into syringes, subjected to large pressures or high temperatures, and extruded out of a nozzle onto

a surface. However, this technique also has limitations with the high levels of shear stress and high temperatures associated with the extrusion process damaging cells and other biological components incorporated into the bioink[23]. Furthermore, extrusion-based printing techniques commonly use microgel particles with diameters from 30-200 μm to avoid small needle gauges that would further increase the shear stress that occurs during printing and printing with particles composed of pNIPam has yet to be explored[18,20,21]. Therefore, other printing techniques that are less damaging to cells, as well as added biological components, and can also be used to print significantly smaller particles need to be explored.

There are techniques used in other industries that have the potential to be adapted for the purpose of creating microgel-based scaffolds and solve the limitations presented by LBL approaches and other printing techniques. One such technique, termed ultrasonic microplotting, has been successfully used in the circuit industry to create flexible circuits[24–26], artificial cells[24], biosensors[28,29], microlenses[30], and carbon nanotube transistor circuits[31,32]. This technique uses a piezoelectric element attached to a glass capillary write head to print inks onto a surface in a non-contact manner. When the piezoelectric element is operational, an ultrasonic wave changes the surface tension and wetting behavior between the resident ink and dispensing tip, causing a bead of ink (meniscus) to form at the dispensing tip, which is brought into contact with the substrate and preferentially wets and "prints onto" the desired substrate. This results in a printing process that does not require the high heat, temperatures, or pressures that are commonly found in other scaffold fabrication techniques, such as electrospinning, certain lithography methods, and extrusion-based printing, which have the potential to damage the material being used and often restricts the inclusion of biological molecules. Moreover, ultrasonic microplotting can achieve picoliters printing for

materials with viscosities up to 500 cP, and for ideal material substrates, higher viscosity inks (> 1200 cP) can also be printed.

This technique is perfectly suited for use in conjunction with microgel particles as the ink can be composed of a suspension of the pre-polymerized colloidal particles which is more amenable to printing using this ultrasonic technique than a polymerized bulk hydrogel. While ultrasonic microplotting holds promise as a technique used in printing hydrogel-based materials for regenerative medicine applications, it has yet to be transitioned from printing circuits and biosensors to printing hydrogel materials. Therefore, in this paper we explore the potential use of the ultrasonic microplotting technique as a method to print patterned microgel films in order to solve some of the limitations in the LBL film fabrication technique, as well as other printing methods.

Materials and Methods:

Microgel bioink synthesis: Microgel particles were created using a precipitation-polymerization reaction. Poly(N-isopropylacrylamide) (pNIPam), N,N'-methylenebis(acrylamide) (BIS), and Acrylic Acid (AAc) were added to 95 mL of de-ionized water to create a final solution with a concentration of 140 mM. The reaction solution was comprised of 91% poly-NIPam, 4% BIS, and 5% AAc. 0.5 mM of sodium dodecyl sulfate (SDS) was added to control for particle size. The solution was then filtered and added to a three-necked reaction vessel that had a nitrogen source, a condenser, and a thermometer attached to it. The solution was heated to 70 °C and allowed to reach thermal equilibrium for 1 hour while under the flow of nitrogen gas and mixing at 450 RPM. Once thermal equilibrium was achieved, a 1 mM solution of ammonium persulfate (APS) was added to initiate the reaction. The reaction was allowed to proceed for 6 hours and cooled overnight

while continuously stirring at 450 RPM. To remove any large aggregates, the cooled solution was filtered using glass wool. Dialysis against deionized water (diH20) was then performed using 1000 kDa tubing (Spectrum Laboratories). Water for dialysis was changed every 12-16 hours over the course of 48 hours. The microgel solution was then lyophilized and reconstituted in diH20 at a stock concentration of 5 mg/mL. Bioinks were then created by diluting the stock concentration to either 2, 0.2, or 0.02 mg/mL and adding either 5%, 10%, or 20% low molecular weight polyethylene glycol 400 (PEG, M_w=380-420 g/mol) by volume.

Bioink microplotting surface functionalization: Glass slides were first cleaned in a sonicator for 15 minutes in each of the following solutions: Alconox® diluted 3:100 in diH_2O, diH_2O, acetone, absolute ethanol, and isopropyl alcohol. The glass slides were then washed twice with deionized water, dried with nitrogen, and functionalized with one of the following: (3-Aminopropyl)triethoxysilane (APTMS), Polyethylenimine (PEI), or bovine serum albumin (BSA). For APTMS functionalization, a 97% (v/v) solution of APTMS was diluted 1:100 into absolute ethanol. The clean glass slides were then covered with the diluted APTMS solution and shaken at room temperature for 2 hours. For functionalization with either PEI or BSA, PEI or BSA were diluted into diH_2O to 0.05 monomolar or 1% by weight (w/v), respectively. The clean glass slides were then covered with either the PEI or BSA solution and incubated overnight at 4°C. Following incubation, the slides were washed twice with diH_2O and allowed to dry.

Bioink microplotting surface contact angle analysis: Contact angle measurements were taken using a Rame-Hart Advanced Contact Goniometer – Model 102. DropImage Advanced software was used to image the water droplets on all of the functionalized glass slides mentioned above. In order to measure the contact angle, a line tangent to the corner of the liquid droplet is drawn and the angle that the tangent makes with the horizontal surface is measured. A contact angle is

measured on each side of the droplet and averaged together to obtain the overall contact angle for the droplet. The solutions used to create a droplet on each of the functionalized surfaces are diH_2O and microgel solutions at either 2, 0.2, or 0.02 mg/ml with either 0%, 5%, 10%, or 20% PEG (v/v).

Bioink microplotting: The patterns used for printing of the microgel bioinks were designed using the SonoDraw GIX II software and can be seen in Figures 2A and 6A. All patterns were printed using a 20, 50, or 100 μm micropipette tip fabricated using G-1 glass capillary tubes, a Narishige PC-10 micropipette puller, and cut using a Narishige MF-900 microforge. The micropipette tips were then superglued onto a piezoelectric element and fit into the holder on the Sonoplot GIX Microplotter II. The printing pattern created in the SonoDraw software was then uploaded to the Sonoplot printing software. Microgel bioinks containing either 0.02, 0.2, or 2 mg/mL of microgel particles and either 5%, 10%, or 20% PEG (v/v) were then created and used for printing the created pattern.

Microplotted microgel film characterization: The printed microgel films were imaged using an EVOS FL Auto (ThermoFisher) and print parameters such as printed dot radius, printed dot circularity, line width, line length, and the percent of the template pattern to print successfully was measured in ImageJ in order to assess print quality and presented as the mean value ± the standard deviation. The percent of the template pattern to print successfully was measured by calculating the total print distance of the template pattern used and then dividing the total print distance for each condition by that value. A total of 3 different prints were imaged with at least 50 dots and 10 lines measured on each print. The thicknesses of the microgel films was determined using a MFP-3D atomic force microscope (AFM; Asylum) in AC mode with ARROW-NCR cantilevers, with a pyramidal tip geometry, and a cantilever constant of 42 N/m, (Nano and More USA). 3 different

line thicknesses were measured on 3 different prints for a total of 9 line widths measured and heights are presented as the mean ± the standard deviation.

Microplotting patterned microgel films: Microgel particles were labeled as either red or green by coupling Alexa Fluor 594 Cadaverine or Alexa Fluor 488 Cadaverine (Thermo Fisher Scientific) to the AAc in the particles through N-ethyl-N′ -(3-(dimethylamino)propyl)carbodiimide (EDC)/ N-hydroxysuccinimide (NHS) coupling chemistry. Patterns with the 2 different microgel formulations were made in SonoDraw and can be seen in Figure 7. The red labeled microgel bioinks were printed first, allowed to dry for 1 hour protected from light, and then the green microgel bioinks were printed. During the printing process the surface that the films were printed on was not moved in order to ensure the precise alignment of the 2 separate print patterns. After printing the patterned films were imaged using an EVOS FL Auto in both the red, green, and phase contrast channels. A minimum of three separate prints per pattern were analyzed. The separate channels where then composited in ImageJ to qualitatively assess the overlap between the red and green microgel bioinks.

Statistical Analysis: All statistical analysis was performed in the Prism software (Graphpad). Data was statistically analyzed using either a one-way or two-way ANOVA with subgroup comparisons done using the Tukey post-hoc test at a 95% confidence interval. All results are reported as the mean ± the standard deviation. * $p<0.05$, ** $p<0.005$, *** $p<0.0005$, **** $p<0.00005$

A

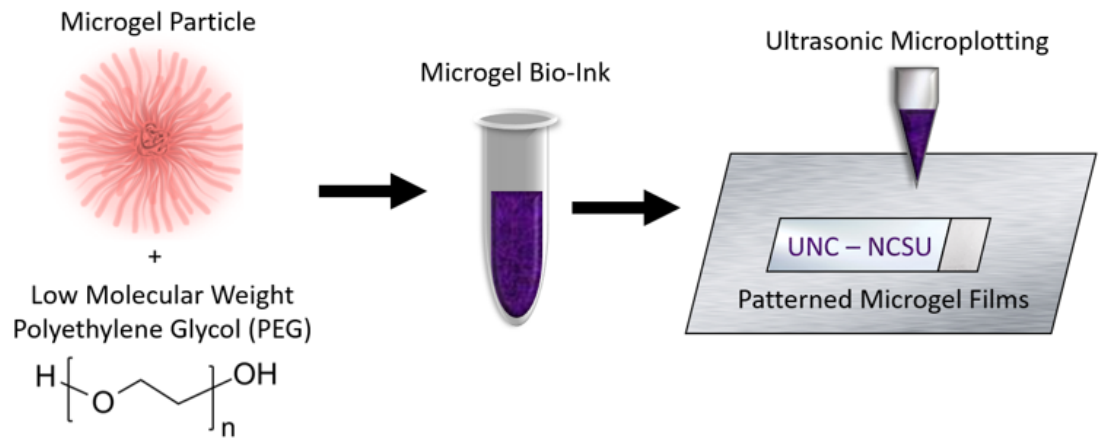

B

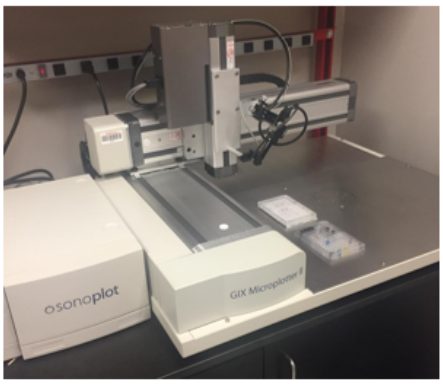

C

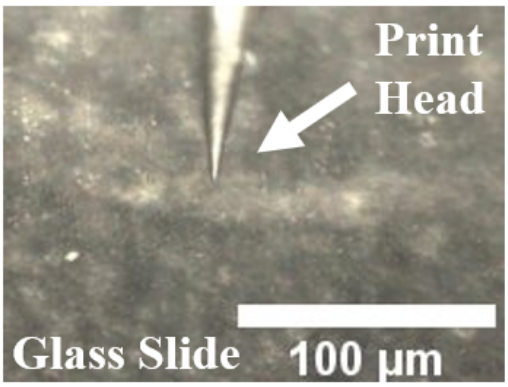

D

Ultrasonic Microplot Print Parameters			
Microgel Concentration (mg/mL)	PEG Concentration (v/v %)	Glass Surface Coating	Print Head Diameter (µm)
0.02	5	No Coating	20
0.2	10	APTMS	50
2	20	PEI	100
		BSA	

Figure 1. Microgel Bio-ink Formulation and Printing Parameters: A) Microgel particles were synthesized in a precipitation-polymerization reaction and mixed with low molecular weight polyethylene glycol in order to make microgel based bioinks used for ultrasonic microplotting. B) Ultrasonic microplotting was performed using a Sonoplot GIX Microplotter II. C) Printing was

performed by using a glass capillary write head on a glass surface. D) Ultrasonic microplotting print parameters were changed by controlling microgel concentration, PEG concentration, the surface coating of the glass to be printed on, and the diameter of the glass capillary.

Results:

Characterization of bioink composition contribution to print quality

To characterize the ability of the ultrasonic microplotting technique to print microgel films, various printing parameters were altered and print quality was then analyzed; specifically the influence of bioink microgel particle concentration, bioink PEG concentration, print surface contact area, and glass capillary write head diameter on print quality were investigated (**Fig. 1**). First, bioink microgel and PEG concentrations were varied while surface contact angle and capillary diameter were kept constant by using clean glass slides and print capillaries 50 μm in diameter. Bioinks with microgel concentrations of 0.02 mg/mL, 0.2 mg/ mL, or 2 mg/mL and PEG concentrations of 5%, 10% or 20% (v/v) were used for printing. A pattern containing dots, lines, filled in shapes, and lettering was developed in order to test the quality and resolution of the resulting prints using each bioink formulation (**Fig. 2A-B, Sup. Fig. 1, Sup. Fig. 2, Sup. Fig. 3**). Each print was imaged and parameters including printed dot radii and circularity, printed line width and length, and the percentage of the template pattern to successfully print were measured (**Fig. 2C-G**) to evaluate the overall print quality. As the microgel and PEG concentration increased, the dot radii, line width, and line length all increased with the 2 mg/mL and 20% PEG (v/v) bioink having mean values of 76.2±7.8 μm, 127.9±5.0 μm, and 1,172.1±18.9 μm, respectively. Also, the only ink formulations where 100% of the template pattern printed successfully were those with the highest microgel and PEG concentrations.

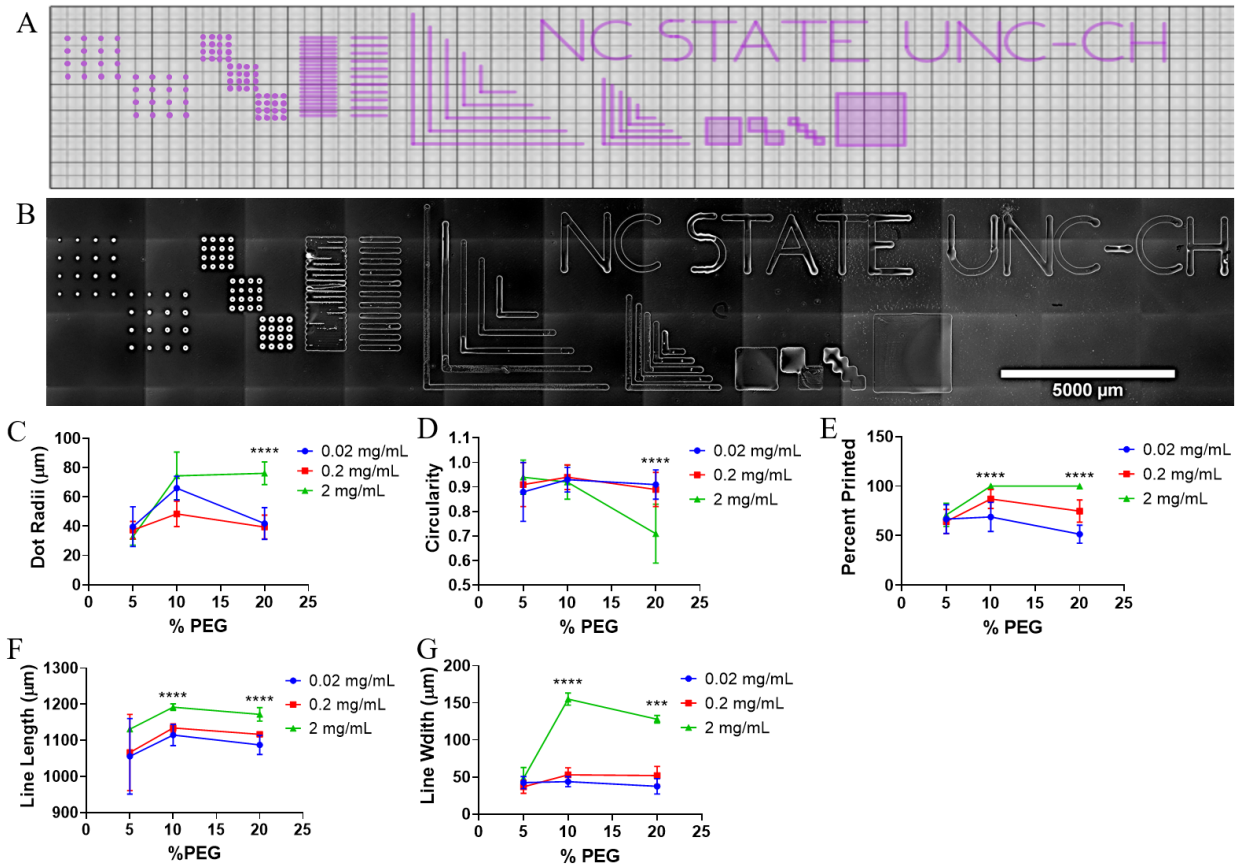

Figure 2. Print Quality Resulting from Bioinks with Changing Microgel and PEG Concentrations on Plain Glass: A) A template pattern was designed with several different features including dots, lines, filled in shapes, and curves in order to capture as many differences in print quality. B) A representative print image from the bioink containing 2 mg/mL of microgel particles and 20% PEG (v/v). C-G) Print quality was assessed by measuring features in ImageJ such as dot radii, circularity, the percent of the template pattern to print, printed line length, and printed line width respectively. Significant differences were measured between microgel bioinks with different microgel concentration, but the same percentage of PEG. *** $p<0.0005$, **** $p<0.00005$

Film thickness is another indicator of the print quality such that a thicker film indicates a higher quality print. To measure film thickness, dry AFM imaging was performed on printed lines created

using the various bioink formulations characterized above (**Fig. 3A**). AFM heights show that at the highest microgel concentration of 2 mg/mL, the thickest print of 1.9±0.3 μm occurred when the PEG concentration was also at its highest value of 20% by volume, as those prints were significantly thicker ($p<0.0005$) than the prints created using a bioink of 2 mg/mL and either 10% or 5% PEG that had thicknesses of 1.3±0.3 μm and 0.4±0.2 µm, respectively (**Fig. 3B**). Subsequently, even at the highest PEG concentration of 20% by volume, the thickest print of 1.9±0.3 μm occurred when the concentration of microgels in the bioink was at its highest value of 2 mg/mL. Prints produced with bioinks comprised of 20% PEG and 2 mg/mL microgels were significantly thicker ($p<0.0005$) than the prints created using a bioink of 20% PEG and 0.2 or 0.02 mg/mL of microgel particles which had thicknesses of 0.4±0.1 µm and 0.3±0.1 µm respectively (**Fig. 3C**). Taken together, the results from the print quality analysis and print thickness measurements show that both the concentration of the microgels and PEG in the bioink are important factors in determining the overall print quality, with the prints with the highest quality, that were also the thickest, occurring with a bioink composition of 2 mg/mL and 20% PEG.

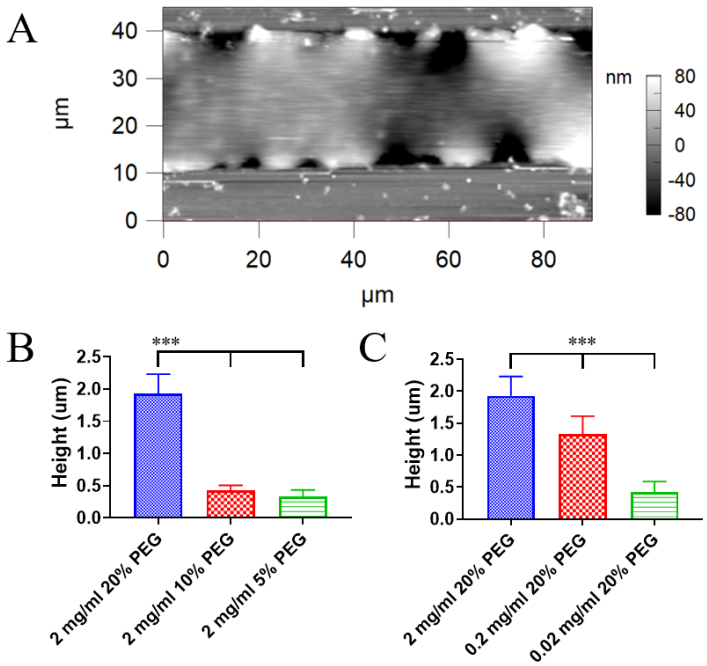

Figure 3. Microgel Bioink Print Heights Measured by Atomic Force Microscopy: Atomic force microscopy (AFM) was used in order to determine the thickness of printed lines made on plain glass with bioinks containing different microgel and PEG concentration. A) A representative image of a printed line as imaged by AFM. B) The heights of printed lines measured by AFM where microgel concentration remained constant at 2 mg/mL and PEG percentage was changed. C) The heights of printed lines measured by AFM where PEG percentage remained constant at 20% and microgel concentration was changed. *** $p<0.0005$

Contact angle analysis

Subsequent studies focused on determining how altering the print surface influenced print quality. Print surfaces included glass slides modified with PEI, APTMS, or BSA. Prior to printing on these surfaces, contact angle analysis of the microgel bioink on the coated surfaces was performed. It was found that changing either the PEG concentration while the microgel concentration was held constant or changing the microgel concentration while the PEG concentration was held constant had little effect on the resulting contact angle (**Fig. 4F-G, Sup. Fig. 4**). Average contact angles of 50.8°±6.3°, 54.4°±3.1°, 65.2°±0.2°, and 77.5°±3.6° were measured for clean glass, PEI coated glass, APTMS coated glass, and BSA coated glass, respectively. The only statistical differences ($p<0.05$) found were between bioinks comprised of 5% PEG (v/v) and 20% PEG (v/v) with 2 mg/mL microgels on the clean glass surface and between bioinks comprised of 0.02 mg/mL and the 0.2 mg/mL or 2 mg/mL with 20% PEG (v/v) on the PEI coated surface. All other conditions within each surface were not statistically different. However, the contact angle of the surface did change significantly ($p<0.05$) with each different surface coating. Using a microgel bioink composition of 2 mg/mL and 20% PEG (v/v), the clean glass surface had the lowest contact angle of 49.0±6.0, the PEI coated surface had a contact angle of

56.5°±1.6°, the APTMS coated surface had a contact angle of 62.8°±1.5°, and the BSA coated surface had the highest contact angle of 75.0°±5.9° (**Fig. 4H**). Overall, contact angle analysis showed that bioink formulation did not have a huge impact on the resulting contact angle, but contact angle could be controlled by changing the type of surface coating on the glass slide.

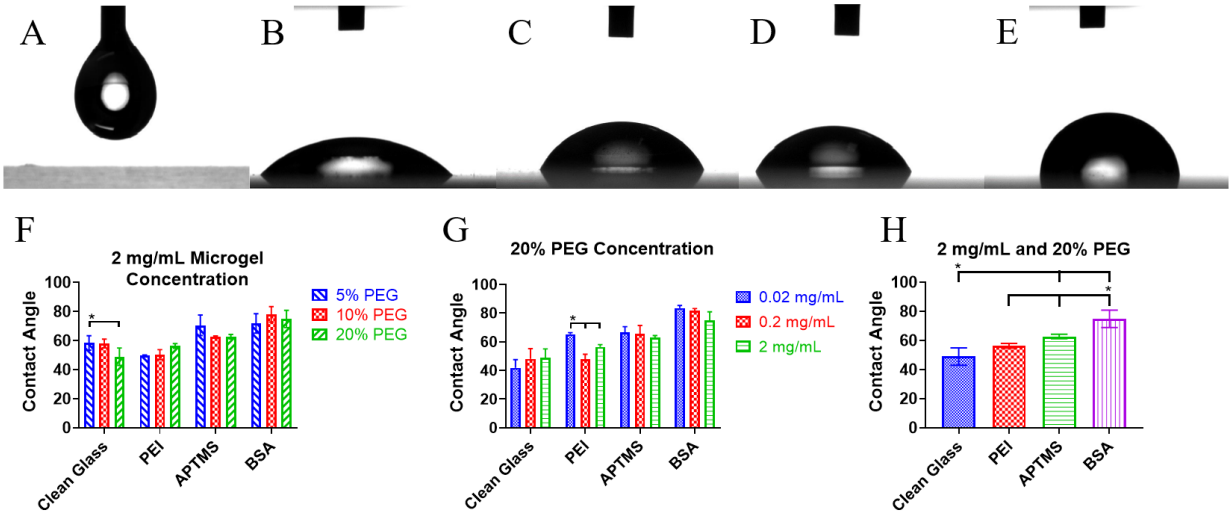

Figure 4. Microgel Bioink Contact Angle Changes Based on Surface Coating: A) Contact angle measurements were taken using a Rame-Hart Advanced Contact Goniometer – Model 102 and DropImage Advanced software was used to image the water droplets. B-E) Representative droplet images for clean glass surfaces, PEI coated surfaces, APTMS coated surfaces, and BSA coated surfaces respectively. F) Contact angle of bioink droplets where microgel concentration was kept constant at 2 mg/mL and PEG concentration was varied. G) Contact angle of bioink droplets where PEG percentage was kept constant at 20% and microgel concentration was varied. H) Contact angle of bioinks with 2 mg/mL of microgels and 20% PEG. * $p<0.05$

Analysis of influence of contact angle on print quality

In these studies, bioink composition was kept constant while print surface was varied. Printing with a bioink of 2 mg/mL microgel particles and 20% PEG (v/v) on the coated surfaces resulted

in a biphasic response between contact angle and print quality (**Fig. 5, Sup. Fig. 5**). With increasing contact angle, the quality of the printed dots behaved as expected with dot radii decreasing to a value of 39.3±1.6 μm and dot circularity increasing to 0.96±0.04 on BSA coated surfaces (**Fig. 5B-C**). However, line width and line length followed a biphasic response and decreased to their lowest values of 27.9±5.5 μm and 1078.6±16.3 μm, respectively, on the APTMS surface, but increased to a value of 79.3±3.0 μm and 1117.3±10.6 μm, respectively, on the BSA surfaces (**Fig. 5E-F**). Also, the APTMS coated surface was the only surface to not print 100% of the template pattern, while the BSA coated surface, at a higher contact angle, did (**Fig. 5D**). The printed line thickness also varied with contact angle as the thickness was greatest on the clean glass and APTMS coated surfaces with values of 1.9±0.3 μm and 1.6±0.2 μm, respectively, while the PEI and BSA coated surfaces had significantly thinner ($p<0.005$) printed lines, having thickness values of 1.0±0.2 μm and 1.0±0.1 μm, respectively. These results show that contact angle does play an important role in print quality. However, due to the biphasic response observed, it is possible that other surface properties also influence print quality.

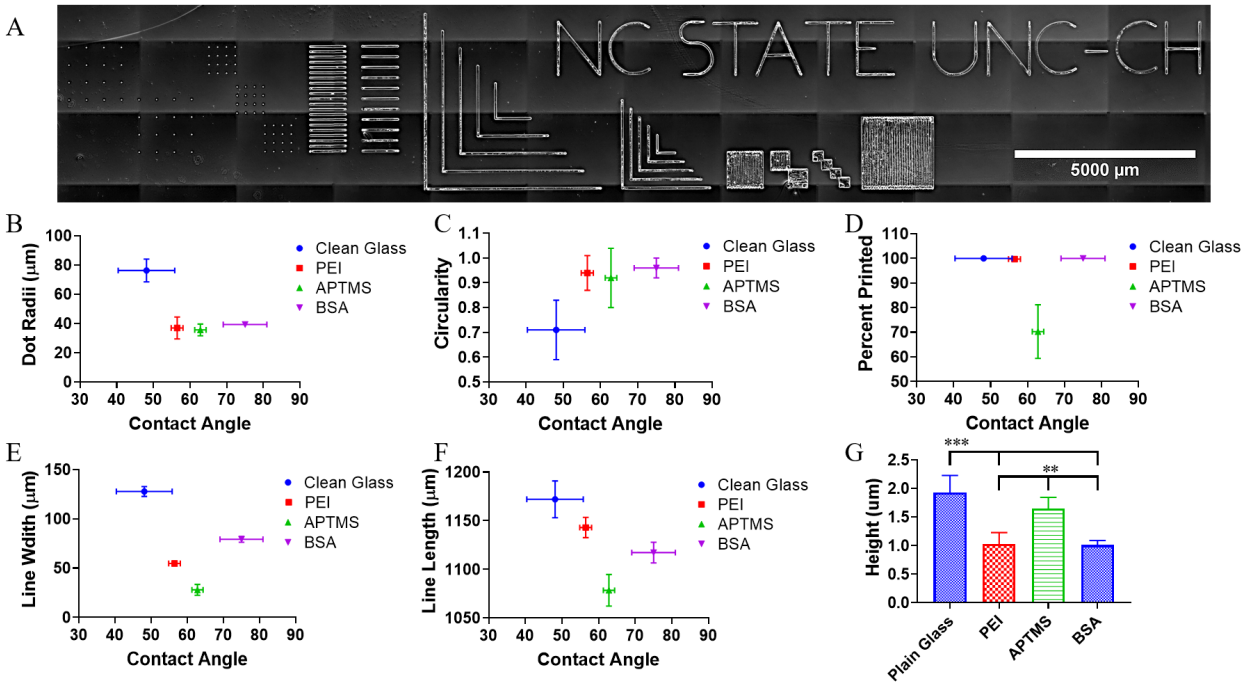

Figure 5. Changing Surface Coating Effects Microgel Bioink Print Quality: A) Representative image of a bioink containing 2 mg/mL of microgels and 20% PEG on a BSA coated surface. B-F) Print quality on each coated surface using a bioink containing 2 mg/mL of microgels and 20% PEG was measured in ImageJ by analyzing printed dot radii, printed dot circularity, the percent of the template pattern to print, printed line width, and printed line length respectively. G) The heights of printed lines measured by AFM. ** $p<0.005$, *** $p<0.0005$

Influence of print head diameter on print quality

Next, the influence of the diameter of the glass capillary print head on print quality was analyzed. Glass capillary print head diameters of 20 µm, 50 µm, or 100 µm were investigated while the contact angle of the surface was held constant by printing on BSA coated slides (**Fig. 6A-B, Sup. Fig. 6**). Bioink formulation was also kept constant at 2 mg/mL microgels and 20% PEG (v/v). While printing parameters appeared to change linearly with increasing capillary diameter, print quality appeared to be the highest with the intermediate diameter capillary. Dot radii, line width,

and line length all significantly ($p<0.0005$, $p<0.005$, and $p<0.0005$ respectively) increased with increasing capillary diameter, with the highest values of 90.7±4.1 µm, 138.7±19.4 µm, and 1705.6±27.7 µm respectively occurring with the largest tip diameter of 100 µm (**Fig. 6C,F,G**). However printing with the 50 µm diameter capillary, led to significantly higher ($p<0.05$) dot circularity values compared to the 100 µm diameter capillary and a significantly greater ($p<0.05$) percentage of the template pattern to print successfully compared to the 20 µm diameter capillary, having values of 0.96±0.04 and 100±5% respectively (**Fig. 6D,E**). While changing the tip diameter does increase the print feature size, there is a tradeoff in quality, as seen by the decrease in printed dot circularity and the increase in printed line length and width, resulting in the 50 µm diameter tip having the best overall print quality.

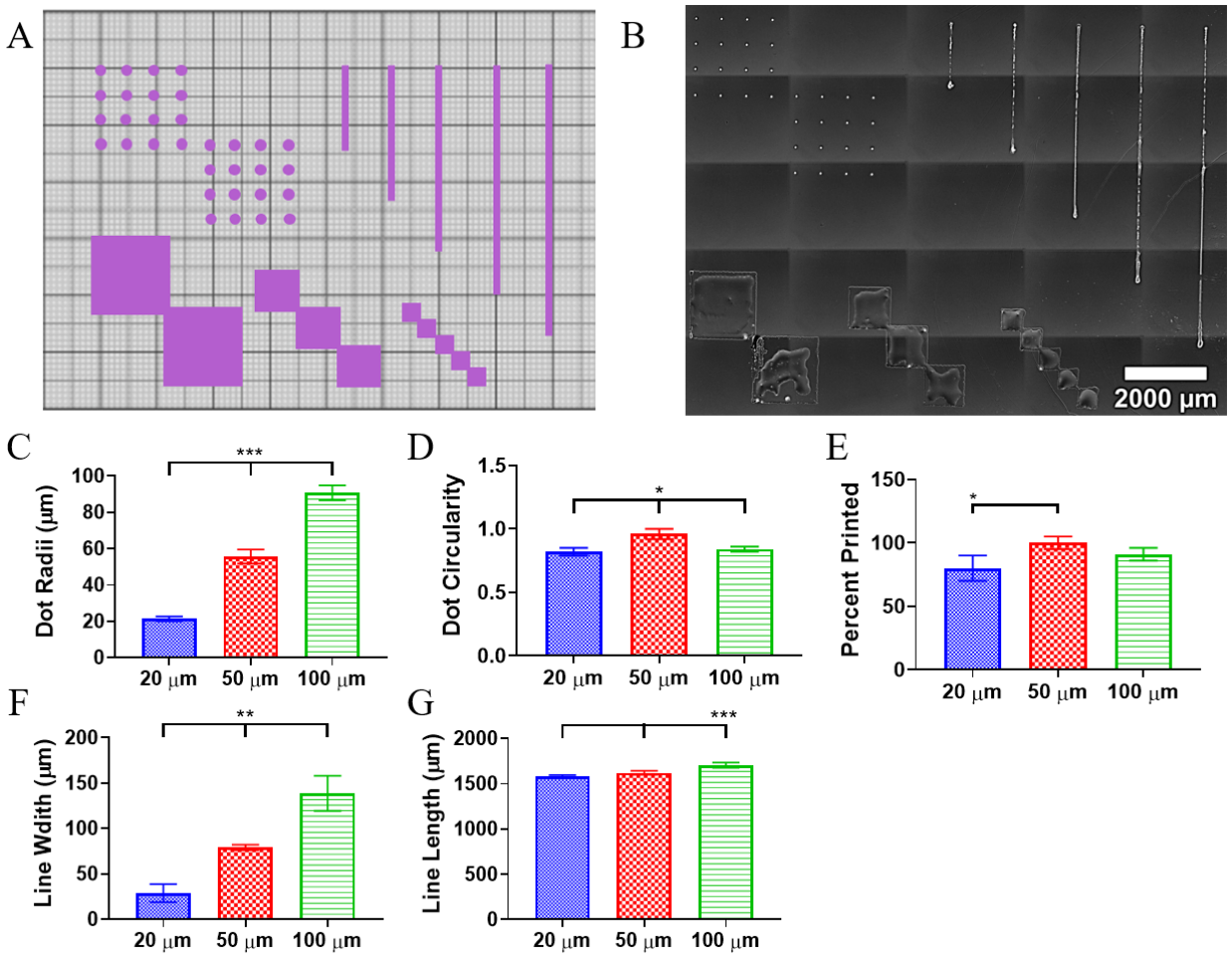

Figure 6. Printing Features Increases Linearly with Changing Print Head Diameter: A) A template pattern was designed in order to measure how printed feature quality changed with the glass capillary print head diameter. B) A representative image of a print using a 50 μm diameter with a bioink containing 2 mg/mL of microgels and 20% PEG on a BSA coated surface. C-G) Print quality was measured in ImageJ by analyzing printed dot radii, printed dot circularity, the percent of the template pattern to print, printed line width, and printed line length respectively. * $p<0.05$, ** $p<0.005$, *** $p<0.0005$

Printing patterned microgel films

Having established an initial understanding of how changing each parameter affects print quality, studies were initiated to evaluate the feasibility of patterning microgels with varied composition. To that end, patterned microgel films were printed using either red labeled or green labeled microgel particles at a concentration of 2 mg/mL with 20% PEG on BSA coated surfaces. To test the resolution capabilities while printing multiple microgel bioinks on the same surface, patterns with features of either 200x200 μm, 100x100 μm, 50x100 μm, or 50x50 μm were created (**Fig. 7**). For the patterns with feature sizes of 200x200 μm and 100x100 μm, the spaces where the green microgels are to be printed next to the red microgels are highly defined indicating that this technique can easily print patterns with a feature size resolution of 100-200 μm. As the pattern features decrease in size to island sizes of 50x100 μm, there are defined spaces in the red channel where the green microgels are going to be printed however they are not as defined as the patterns with the larger feature size. Lastly, as feature size decreases to the pattern where island sizes are 50x50 μm in size, the spaces where the green particles are to be printed are not as defined and it appears that the red labeled microgels fill in that space to a greater degree. Based on these results, it appears that resolution capabilities are limited to around 50-100 μm in size as it is somewhere

between an island size of 50x100 μm and 50x50 μm where it is not possible to print areas of differing microgels next to one another without overlap.

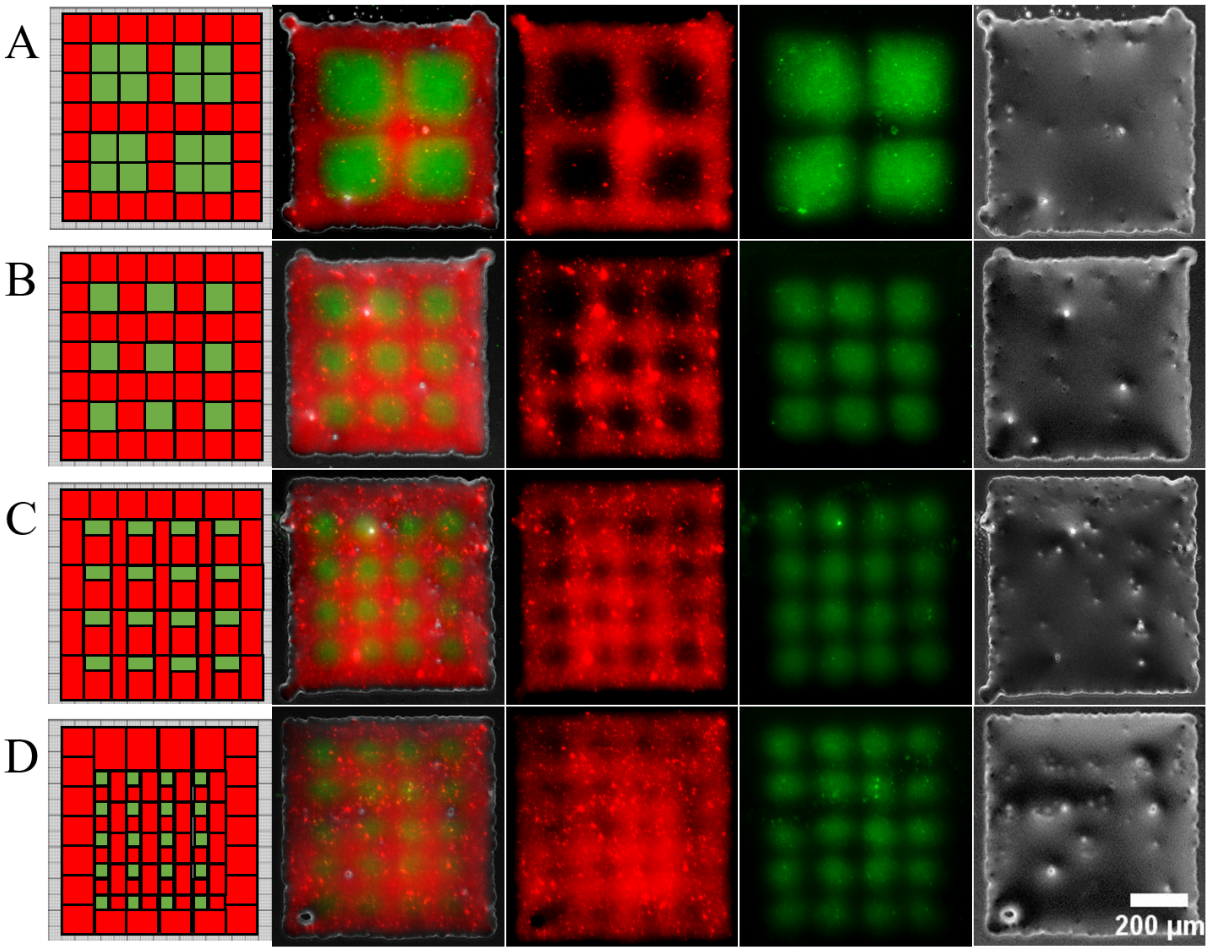

Figure 7. Patterning Microgel Films Using an Ultrasonic Microplotter: Patterned microgel films were created using particles labeled with Alexa Fluor 594 Cadaverine (red) or Alexa Fluor 488 Cadaverine (green). Bioinks with the labeled particles were created at a concentration of 2 mg/mL and printed on BSA coated surfaces. Patterns with green feature sizes of 200x200 μm (A), 100x100 μm (B), 50x100 μm (C), and 50x50 μm (D) were printed.

Discussions and conclusions:

In this work, we investigate the utility of ultrasonic plotting in creating patterned pNIPAm scaffolds. In order to understand how user controlled parameters effect printing quality, bioink

formulation, contact angle of the surface, and print head diameters were varied independently of one another. The first set of parameters that was varied during the printing process was the microgel bioink composition. The bioink is composed of microgel particles and low molecular weight polyethylene glycol 400 (PEG). PEG is a common additive in bioink material blends due to its ability to increase the mechanical property of the resulting material[33,34]. PEG is also used as a lubricant in many 3D printing applications in order to aid the loading and dispensing process[35–38]. This increases the ability of the bioink to print successfully while also preventing clogging of the write head; for these reasons, PEG was included in the bioinks here. Results showed that increasing bioink PEG concentration and bioink microgels concentration, while holding other parameters constant, resulted in increasing print quality. Bioinks comprised of 2 mg/mL with 20% PEG (v/v) were found to have the overall highest print quality, as evidenced by results demonstrating prints with this bioink have the largest and thickest print features while also successfully printing 100% of the template pattern. Indeed, our results show that the addition of PEG does aid printing by increasing the wetting of the bioink on the glass surface due to the lubrication properties of the PEG aiding the dispensing process. It is important to note that similar results could have been achieved with using higher molecular weights of PEG in lower amounts, however higher molecular weights would be harder to remove from the dried printed microgel films which is why a low molecular weight was used. Next, the influence of surface contact angle on print quality was analyzed, while keeping other printing parameters constant, by coating glass slides with PEI, APTMS, or BSA. The surface coatings were chosen based off typical microgel film LBL fabrication, which uses APTMS to functionalize the glass and PEI which is used to electrostatically hold microgel layers together, and the potential for cell culture, where BSA would prevent non-specific cell adhesion and thereby promote adhesion to the printed microgels. Contact angle

analysis showed that clean glass had the lowest contact angle, PEI and APTMS had an intermediate contact angle, and BSA had the highest contact angle. Initially, it was hypothesized that contact angle would influence print quality, with quality increasing as contact angle increased, due to an increase in the hydrophobicity of the surface which would prevent the print from spreading and increase resolution. Indeed, this hypothesis holds when printing dots as both the dot radii and dot circularity increased with increasing contact angle as expected. However, this hypothesis did not hold with regards to printed line length, width, and the percent of the template to print successfully. In fact, it appears that there is a biphasic response resulting in APTMS having the lowest print quality even though it is at an intermediate contact angle value. These results indicate that there could be other surface parameters that impact microgel bioink print quality. Surface charge and magnitude may be contributing to these results as both PEI and APTMS are positively charged, with APTMS having a higher charge magnitude than PEI, and BSA having a negative charge, but further tests would need to be performed in order to substantiate this hypothesis. Overall, the results from changing the contact angle showed that either the BSA or PEI coated surfaces represent the best print substrates, as evidenced by results demonstrating that prints on these surfaces have print features closest to the diameter of the write head with 100% of the template pattern successfully printed.

Finally, the influence of glass capillary print head diameter on print quality was analyzed while holding all other printing parameters constant. The diameter of the print head influences the size of the printed features; we hypothesized that smaller diameters would correlate with greater print resolution. Results demonstrated that print feature size increased linearly with increasing capillary diameter; dot radii, line width, and line length all increased with an increase in tip diameter. However, this change in resolution comes at the expense of the overall print quality. As the tip

diameter decreased, the percent of the template pattern printed also decreased. This could be caused by partial clogging of the smaller tip diameters with the microgel particles in the bioink or it could be that the volume wicking onto the surface from the capillary was not large enough to maintain a continuous flow over the size of the pattern. In order to increase the resolution further, the microgel bioink formulation might need to be altered or perhaps the design of the pattern needs to be proportionately scaled to the tip diameter.

The goal of this project is to spatially control deposition of microgels to create scaffolds with exquisitely controlled mechanical, adhesive, and bioactive properties. Previous studies with pNIPAm particle have shown that particle stiffness can be controlled between 3-120 kPa[39], film viscoelasticity can be controlled between a loss tangent of 0.8 and 1.5[16], and bioactivity can easily be achieved through the inclusion of antibodies or targeted peptides[40–42]. This ultrasonic printing technique, therefore, could be used to pattern particles with different properties consistent with the desired application. By optimizing printing parameters, it was possible to create patterned films with a feature size resolution of ~50 μm by using a microgel bioink comprised of 2 mg/mL of microgel particles and 20% PEG (v/v) while printing on a BSA coated surface using a print head diameter of 50 μm. Therefore, this printing technique successfully addressed the major issue of lack of spatial control of LBL methods for microgel scaffold fabrication. This work also opens the door for the development of new and complex microgel platforms that can pattern specific substrate parameters to localized area that are on a similar length scale to a cell's native microenvironment.

While this technique offers huge advantages in 2D film creation, the technology needs further optimization to facilitating printing larger three-dimensional scaffolds. However, results shown here offer promise for extending ultrasonic printing to 3D. Compared to extrusion-based printing,

ultrasonic printing offers higher spatial resolution and a greater degree of control over material properties. The resolution for feature size of most extrusion-based printing methods is between 200-2000 μm[5,17–19,43]. In order to achieve higher resolutions through extrusion-based printing, stiffer or more viscous materials need to be used. A resolution lower than 200 μm has been seen with extrusion-based printing, however this required the use of a material with a stiffness between 100-500 kPa which is greater than the physiological values of most tissues[35]. Using this method, it was possible to print features down to 50 μm with the possibility of even printing at a higher resolution with further optimization. Because the bioinks used in this study are made of microgel suspensions, the mechanical and rheological behavior of the bioink will be governed by the solvent in which the particles are dissolved,[22] meaning that resolution size is independent of the microgel particle mechanical properties. Therefore, it is possible to still achieve a high degree of resolution even with particles that have mechanical properties over a wide range of physiologically relevant values. Overall, this technique offers advantages in 2D film creation as compared to traditional LBL techniques and offers potential advantages in 3D with further development of the technology.

Supporting Information: The following file is available free of charge as a PDF and includes the representative images of microgel printing conditions that are shown in the main text as data points in graphs. These conditions include: bioinks with compositions of either 0.02, 0.2, or 2 mg/ml with either 5%, 10%, or 20% PEG, contact angle analysis of bioinks with compositions of either 0.02 or 0.2 mg/ml with either 5%, 10%, or 20% PEG, bioinks printed on APTMS and PEI coated surfaces, and bioinks printed with a 20 μm or 100 μm capillary write head.

***Corresponding Author:** Ashley C. Brown, PhD

Joint Department of Biomedical Engineering

North Carolina State University and University of North Carolina at Chapel-Hill

911 Oval Drive

4204B Engineering Building III

Raleigh, NC 27606

(919) 513-8231

aecarso2@ncsu.edu

Author Contributions

D.C wrote and edited the manuscript, created bioink formulations, designed and performed experiments, and analyzed data. P.T. created bioink formulations, designed and performed experiments, and analyzed data. T.N. performed all contact angle measurements. M.D. edited the manuscript, designed experiments, and analyzed data. A.C.B. wrote and edited the manuscript, designed experiments, and analyzed data. All authors have given approval to the final version of the manuscript.

Funding Sources

Funding for this project was provided by NSF CMMI 1825398 as well as NCSU's CMI SIRI program, and NCSU's Abram's Shcolar Program.

Acknowledgments

The authors would like to acknowledge Mike Wilkins for his help with both the Sonoplot and Narishige micropipette equipment and Matthew Nordberg for his help with preparing microgel bioinks and printing surfaces.

Abbreviations

AAc, acrylic acid; AFM, atomic force microscopy; APS, ammonium persulfate; APTMS, (3-Aminopropyl)triethoxysilne; BIS N,N'-methylenebis(acrylamide); BSA, bovine serum albumin; diH2O, deionized water; EDC, N-ethyl-N′ -(3-(dimethylamino)propyl)carbodiimide; LBL, layer-by-layer; NHS, N-hydroxysuccinimide; PEG, low molecular weight polyethylene glycol 400; PEI, polyethylenimine; pNIPam, poly N-isopropylacrylamide; SDS, sodium dodecyl sulfate.

References

1. Sakiyama-Elbert, S. E. & Hubbell, J. A. Functional Biomaterials: Design of Novel Biomaterials. Annu. Rev. Mater. Res. 31, 183–201 (2001).

2. Plamper, F. A. & Richtering, W. Functional Microgels and Microgel Systems. Acc. Chem. Res. 50, 131–140 (2017).

3. Townsend, J. M. et al. Colloidal Gels with Extracellular Matrix Particles and Growth Factors for Bone Regeneration in Critical Size Rat Calvarial Defects. AAPS J. 19, 703–711 (2017).

4. Zhang, H. et al. Direct 3D Printed Biomimetic Scaffolds Based on Hydrogel Microparticles for Cell Spheroid Growth. Adv. Funct. Mater. 30, 1910573 (2020).

5. Martínez Ávila, H., Schwarz, S., Rotter, N. & Gatenholm, P. 3D bioprinting of human chondrocyte-laden nanocellulose hydrogels for patient-specific auricular cartilage regeneration. Bioprinting 1–2, 22–35 (2016).

6. Spears, M. W., Herman, E. S., Gaulding, J. C. & Lyon, L. A. Dynamic Materials from Microgel Multilayers. Langmuir 30, 6314–6323 (2014).

7. Saxena, S. et al. Microgel film dynamics modulate cell adhesion behavior. Soft Matter 10, 1356–1364 (2014).

8. Bachman, H. et al. Ultrasoft, highly deformable microgels. Soft Matter 11, 2018–2028 (2015).

9. Saxena, S., Hansen, C. E. & Lyon, L. A. Microgel Mechanics in Biomaterial Design. Acc. Chem. Res. 47, 2426–2434 (2014).

10. Park, S., Han, U., Choi, D. & Hong, J. Layer-by-layer assembled polymeric thin films as prospective drug delivery carriers: design and applications. Biomater. Res. 22, 29 (2018).

11. Nyström, L. et al. Avidin–Biotin Cross-Linked Microgel Multilayers as Carriers for Antimicrobial Peptides. Biomacromolecules (2018) doi:10.1021/acs.biomac.8b01484.

12. Ma, S. et al. Fabrication of Microgel Particles with Complex Shape via Selective Polymerization of Aqueous Two-Phase Systems. Small 8, 2356–2360 (2012).

13. Xia, Y. et al. Cell attachment/detachment behavior on poly(N-isopropylacrylamide)-based microgel films: the effect of microgel structure and swelling ratio. J. Mater. Sci. 53, 8795–8806 (2018).

14. Gao, Y. Stimuli-Responsive Microgel-Based Systems and Their Application for Controlled Drug Release. ERA (2017) doi:10.7939/R3T14V555.

15. Keskin, D., Mergel, O., Mei, H. C. van der, Busscher, H. J. & Rijn, P. van. Inhibiting Bacterial Adhesion by Mechanically Modulated Microgel Coatings. Biomacromolecules (2018) doi:10.1021/acs.biomac.8b01378.

16. Chester, D., Kathard, R., Nortey, J., Nellenbach, K. & Brown, A. C. Viscoelastic properties of microgel thin films control fibroblast modes of migration and pro-fibrotic responses. Science Direct doi:10.1016/j.biomaterials.2018.09.012.

17. Morgan, F. L. C., Moroni, L. & Baker, M. B. Dynamic Bioinks to Advance Bioprinting. Adv. Healthc. Mater. n/a, 1901798 (2020).

18. Highley, C. B., Song, K. H., Daly, A. C. & Burdick, J. A. Jammed Microgel Inks for 3D Printing Applications. Adv. Sci. 6, 1801076 (2019).

19. Peak, C. W., Stein, J., Gold, K. A. & Gaharwar, A. K. Nanoengineered Colloidal Inks for 3D Bioprinting. Langmuir 34, 917–925 (2018).

20. Kamperman, T. et al. Single Cell Microgel Based Modular Bioinks for Uncoupled Cellular Micro- and Macroenvironments. Adv. Healthc. Mater. 6, 1600913 (2017).

21. Xin, S., Chimene, D., Garza, J. E., Gaharwar, A. K. & Alge, D. L. Clickable PEG hydrogel microspheres as building blocks for 3D bioprinting. Biomater. Sci. 7, 1179–1187 (2019).

22. Daly, A. C., Riley, L., Segura, T. & Burdick, J. A. Hydrogel microparticles for biomedical applications. Nat. Rev. Mater. 5, 20–43 (2020).

23. Hospodiuk, M., Moncal, K., Dey, M. & Ozbolat, I. Extrusion-Based Biofabrication in Tissue Engineering and Regenerative Medicine.

24. Wang, X. et al. Electrical and Mechanical Properties of Ink Printed Composite Electrodes on Plastic Substrates. Appl. Sci. 8, 2101 (2018).

25. Cai, L., Zhang, S., Miao, J., Yu, Z. & Wang, C. Fully Printed Stretchable Thin-Film Transistors and Integrated Logic Circuits. ACS Nano 10, 11459–11468 (2016).

26. Robinson, A. P., Minev, I., Graz, I. M. & Lacour, S. P. Microstructured Silicone Substrate for Printable and Stretchable Metallic Films. Langmuir 27, 4279–4284 (2011).

27. Karzbrun, E., Tayar, A. M., Noireaux, V. & Bar-Ziv, R. H. Programmable on-chip DNA compartments as artificial cells. Science 345, 829–832 (2014).

28. Molazemhosseini, A., Magagnin, L., Vena, P. & Liu, C.-C. Single-use nonenzymatic glucose biosensor based on CuO nanoparticles ink printed on thin film gold electrode by micro-plotter technology. J. Electroanal. Chem. 789, 50–57 (2017).

29. Penkala, K. et al. Graphene-based electrochemical biosensing system for medical diagnostics. in 2017 IEEE 37th International Conference on Electronics and Nanotechnology (ELNANO) 305–309 (2017). doi:10.1109/ELNANO.2017.7939768.

30. Zang, Z., Tang, X., Liu, X., Lei, X. & Chen, W. Fabrication of high quality and low cost microlenses on a glass substrate by direct printing technique. Appl. Opt. 53, 7868 (2014).

31. Li, Q. et al. Designing hybrid gate dielectric for fully printing high-performance carbon nanotube thin film transistors. Nanotechnology 28, 435203 (2017).

32. Chen, P. et al. Fully Printed Separated Carbon Nanotube Thin Film Transistor Circuits and Its Application in Organic Light Emitting Diode Control. Nano Lett. 11, 5301–5308 (2011).

33. Gopinathan, J. & Noh, I. Recent trends in bioinks for 3D printing. Biomater. Res. 22, (2018).

34. Gungor-Ozkerim, P. S., Inci, I., Zhang, Y. S., Khademhosseini, A. & Dokmeci, M. R. Bioinks for 3D bioprinting: an overview. Biomater. Sci. 6, 915–946 (2018).

35. Hinton, T. J. et al. Three-dimensional printing of complex biological structures by freeform reversible embedding of suspended hydrogels. Sci. Adv. 1, e1500758 (2015).

36. Melocchi, A. et al. Hot-melt extruded filaments based on pharmaceutical grade polymers for 3D printing by fused deposition modeling. Int. J. Pharm. 509, 255–263 (2016).

37. Melocchi, A. et al. 3D printing by fused deposition modeling (FDM) of a swellable/erodible capsular device for oral pulsatile release of drugs. J. Drug Deliv. Sci. Technol. 30, 360–367 (2015).

38. Okwuosa, T. C. et al. Fabricating a Shell-Core Delayed Release Tablet Using Dual FDM 3D Printing for Patient-Centred Therapy. Pharm. Res. 34, 427–437 (2017).

39. Hashmi, S. M. & Dufresne, E. R. Mechanical properties of individual microgel particles through the deswelling transition. Soft Matter 5, 3682–3688 (2009).

40. Sproul, E. P., Nandi, S., Roosa, C., Schreck, L. & Brown, A. C. Biomimetic Microgels with Controllable Deformability Improve Healing Outcomes. Adv. Biosyst. 0, 1800042 (2018).

41. Joshi, A., Nandi, S., Chester, D., Brown, A. C. & Muller, M. Study of poly (N-isopropylacrilamide-co-acrylic acid) (pNIPAM) microgel particle induced deformations of tissue mimicking phantom by ultrasound stimulation. Langmuir (2017) doi:10.1021/acs.langmuir.7b02801.

42. Mihalko, E., Huang, K., Sproul, E., Cheng, K. & Brown, A. C. Targeted Treatment of Ischemic and Fibrotic Complications of Myocardial Infarction Using a Dual-Delivery Microgel Therapeutic. ACS Nano 12, 7826–7837 (2018).

43. Webb, B. & Doyle, B. J. Parameter optimization for 3D bioprinting of hydrogels. Bioprinting 8, 8–12 (2017).